Applied Catalysis A: General 391 (2011) 377-385

Structural properties of an unsupported model Pt–Sn catalyst and its catalytic properties in cyclohexene transformation

Z. Paál[1*], A. Wootsch[1], D. Teschner[1,2], K. Lázár[1], I. E. Sajó[3], N. Győrffy[1], G. Weinberg[2], A. Knop-Gericke[2], R. Schlögl[2]

[1] Institute of Isotopes, Hung. Acad. Sci., POB 77, Budapest, H-1525, Hungary
[2] Department of Inorganic Chemistry, Fritz-Haber-Institut der MPG, Faradayweg 4-6, D-14195 Berlin, Germany
[3] Chemical Research Center, Hung. Acad. Sci., POB 17, Budapest, H-1525 Hungary

[*] Corresponding author: e-mail paal@iki.kfki.hu,

Received 4 February 2010; Received in revised form 26 May 2010; Accepted 28 May 2010; Available online 8 June 2010

Abstract

Unsupported PtSn powder was prepared by direct reduction of a solution containing both H_2PtCl_6 and $SnCl_4$ using hydrazine as the reducing agent. The dark gray powder was characterized with Scanning Electron microscopy (SEM), EDX analysis, Mössbauer spectroscopy, X-ray diffraction, XPS depth profiling after different treatments: pre-sintering, O_2 and H_2 treatments. SEM showed a conglomerate of small spherical particles (0.2 – 1.5 μm). They contained Pt, various PtSn alloy phases and tin oxide(s). EDX showed 70-75% Pt and 25-30% Sn on various grains. The mixture of Pt_3Sn and SnO_2 represented the final stabilized state obtained upon repeated heating in air and, finally, H_2. This mixed Pt–Sn was catalytically inactive in "structure-sensitive" reactions, such as methylcyclopentane ring opening or cyclohexane dehydrogenation, but was active in "structure-insensitive" hydrogenation and also in the dehydrogenation of cyclohexene. The relative importance of the latter two reactions depended strongly on the previous treatments of the catalyst – i.e., on its composition, the final stage (Pt_3Sn and SnO_2) being most active, with cyclohexane as the main product.

Keywords: PtSn, bimetallic catalyst, X-Ray diffraction, Mössbauer spectroscopy, XPS, Electron microscopy, hydrogenation and dehydrogenation of cyclohexene,

1. Introduction

Addition of tin to Pt catalysts plays an important role in controlling the activity and selectivity in several different catalytic reactions [1-3]. From the late 1970s Sn-Pt/Al_2O_3 catalysts have been applied in the naphtha reforming industry, in order to improve stability and selectivity towards dehydrogenation, isomerization and aromatization [1-5]. In the last 30 years Sn-Pt system was studied extensively in model hydrocarbon reforming reactions, for example in transformations of cyclohexane [6-8], methylcyclopentane [9], heptane [7] and also hexane [5,10-12]. The Sn-Pt catalytic system could be successfully applied in many different reactions: dehydrogenation of light alkanes [13-15], hydrogenation of 1,3-butadiene [16], selective hydrogenation of α,β-unsaturated aldehydes [17,18] and nitriles [19], selective catalytic reduction of NO_x with hydrocarbons [20], hydrogen-assisted dechlorination reactions [21-23], low-temperature CO oxidation [21,24-28], CO oxidation in the presence of hydrogen (PROX) [29-31], electrocatalytic total oxidation of methanol [32,33] and ethanol [34,35] for direct fuel cell application, and in electrocatalysis for preparation of CO resistant PEMFC anodes [36,37].

To explain the advantageous effect of tin on the properties of Pt catalysts two mechanisms were suggested [1]. The first type of interpretation is the so-called "ensemble" or "geometric" effect. According to this concept, the primary role of tin is the separation and stabilization of platinum ensembles and retaining them in high "dispersion" (i.e., Pt accessibility) [38-40]. Sn is preferentially

deposited on larger Pt ensembles active in hydrogenolysis [6]. This mechanism could explain the increased stability of Sn-Pt catalysts in the refinery. The second interpretation is the so-called "electronic" effect. It emphasizes the modification of electronic density of platinum due to a partial positive charge transfer from Sn^{n+} species and/or different electronic structure in Pt-Sn alloys [29,41-43]. Several characterization techniques, such as electrochemical methods [44], XPS [13,39,44], EXAFS [13], ^{119}Sn Mössbauer spectroscopy [11,21-23,26], suggested strong electronic interaction between Sn and Pt. In different reactions obviously alternative explanations were given account for the catalytic properties of Sn-Pt materials. However, most of the studies agree that the ensemble and electronic effect (including alloy formation) cannot be separated.

The Pt-Sn phase diagram is well established [45] and the enthalpies of formation are known [46]. Five different alloy phases were described [45,46]: $PtSn_4$ orthorombic, $PtSn_2$ cubic, Pt_2Sn_3 hexagonal, PtSn hexagonal and Pt_3Sn centered cubic phase. Among them special catalytic behavior was assigned to Pt_3Sn and partly to PtSn alloy in different reactions, while alloys with higher Sn content were regarded as inactive in most catalytic reactions [11,13,29,30,47]. Modeling by Kappenstein et al. [11] showed that the Pt_3Sn alloy structure has sufficient number of surface Pt atoms that can be active in hydrocarbon transformation. EXAFS and XPS results indicated that PtSn alloys are likely, inactive in isobutene dehydrogenation, they, however, increase the stability of Pt particles without direct contribution in the catalytic reactions [13].

Building up a precise model of the catalyst structure under reaction conditions is, unfortunately, not possible in most of the cases. The Pt loading of supported catalysts is usually 1-5% (or even lower) and the tin modifier is sometimes added in even smaller amounts. ^{119}Sn Mössbauer spectroscopy [11,21-23,26] can reveal the "bulk structure" of metallic particles. Sn^0, Sn^{2+} and Sn^{4+} were identified in Pt/Al_2O_3 [48], their concentration depended on the pretreatment of the catalyst. Exact identification of phases – due to the low Sn loading – is not always possible. The information from XRD studies is rather limited for low metal loadings and for small particles. Even if the "bulk structure" of the supported Sn-Pt samples is unambiguously identified, its surface under reaction conditions might be different [11,26]. X-ray photoelectron spectroscopy (XPS) – one of the most widely used techniques for analyzing catalyst surfaces – has limitations. First, certain difficulties arise for alumina supported Pt, due to the fact that the Pt 4f and Al 2p peaks measured in traditional XPS instruments partially overlap, second, in the case of low metal loading, the surface of metallic particles might be negligible as compared to high surface supports. To overcome these problems, unsupported model catalysts were successfully applied in our earlier studies [49-54]. Pt black is a well-dispersed monometallic catalyst, and can be tested in catalytic reactors, and characterized by bulk techniques, like XRD, as well as by surface-sensitive XPS.

Conventional XPS operates at UHV pressures. Thus, the identification of the weakly adsorbed species and surface structure *during the catalytic run* is difficult (almost impossible). Evacuation induces desorption and/or can change the chemical state of surface species [55-57]. To overcome these limitations, high-pressure XPS chambers were designed already in the late 1970's [55]. A number of high-pressure XPS experiments have been performed since then [58-62]. The in-situ XPS setup used in this study employs differentially pumped electrostatic lenses that allow measurements in a gaseous environment (flow-through mode) at pressures of up to 5 mbar [63-67].

The present paper reports on the preparation of an unsupported Pt-Sn catalyst, by simultaneous direct reduction of both Pt and Sn from a mixed solution (Pt:Sn=3:1) rather than adding Sn to solid Pt. The catalyst was subjected to different treatments, in order to clarify the way of formation and the catalytic behavior of different PtSn alloys. We determined the bulk structure, its surface state and attempted to correlate them with the catalytic properties. Characterization by SEM, EDX, XRD, in-situ, high-pressure XPS, ^{119}Sn-Mössbauer spectroscopy and tests in hydrocarbon reactions are to be reported. Catalytic properties in other reactions (such as PROX) will be published separately.

2. Experimental

2.1. Catalyst preparation and treatments

The PtSn catalyst was prepared by a traditional reduction method [68]. Aqueous hydrazine hydrate solution was added stepwise to a 35% aqueous solution of H_2PtCl_6 and $SnCl_4$ with a nominal atomic ratio of Pt:Sn = 3:1. A dark gray precipitate was formed. That liquid was then heated at 353 K for 24 hours to remove residual ammonia, thereafter it was washed with bidistilled water for several days until reaching neutral pH. The sample was filtered and dried overnight in a vacuum-desiccator over $CaCl_2$ at ~293 K followed by drying in an oven drier at 393 K for 12 hours. This sample is denoted as "PtSn as prepared": **PtSn-AP**. It was then presintered in flowing gas mixture (10% H_2 in He, 30 mL/min at 473 K) for 2 h [49]. According to earlier experiences with unsupported Pt catalysts [52,53,69] this sample is stable and can be stored in air. This sample is called "PtSn presintered": **PtSn-PS**. A fraction of it was pretreated in oxygen for 2 hours at T=573 K (**PtSn-O_2**) and then reduced in H_2 at T=673 K also for 2 hours (**PtSn-H_2**). Reduction in the in-situ XPS apparatus took place at 573 K.

Adsorption properties of the sample were measured after in-situ presintering at 473 K in H_2. Adsorption of H_2 and CO was carried out at room temperature. The Pt accessibility was calculated estimating 1:1 Pt:H_{ads} and Pt:CO_{ads} ratios. Specific surface was determined by N_2 adsorption using the BET method.

Catalytic results were compared with those on an unsupported Pt black sample prepared by the same method using hydrazine, as described previously [49,53,69]. This sample is denoted as **Pt** and after treatments analogous to those applied for Pt-Sn samples **Pt-PS**, **Pt-O_2** and **Pt-H_2**.

2.2. Scanning Electron Microscopy (SEM) and Energy Dispersive Analysis (EDX)

Scanning electron microscopy was measured using FEI Quanta 200F microscope with warm field emission gun. Secondary Electron images were taken with Everhard Thornley Detector (EDT). Energy dispersive analysis (EDX) was measured by EDAX Genesis with Sapphire Detector with Si(Li) crystal and super ultra thin window (SUTW). Images and spectra were taken with accelerating voltages of 10 and 25 kV. Elemental mapping (Sn plus Pt) was performed in a Philips CM200 FEG electron microscope.

2.3. XRD measurements

X-ray powder diffraction scans were measured on a Philips PW 1050/PW 3710 diffractometer equipped with graphite monochromator and proportional counter and using Cu Kα radiation (λ=0.15418 nm). XRD scans were evaluated for quantitative phase composition and crystallite size using a full profile fit method.

2.4. Mössbauer spectroscopy

^{119}Sn-Mössbauer in situ spectra were recorded at 77 K with a constant acceleration KFKI spectrometer equipped with $Ba^{119}SnO_3$ source (300 MBq). The cell was built to allow treatments in various gas atmospheres, with a pellet supported by a thin Be plate [70]. The pellet was made from 172 mg **PtSn-AP** powder diluted with 78 mg Cab-O-Sil (EH5) and pressed with 100 MPa. The sample was pretreated in-situ and measured after all treatments in the **PtSn-PS**, **PtSn-O_2**, and **PtSn-H_2** states, consecutively. The recorded spectra were decomposed to Lorentzian shaped lines. None of the positional parameters were initially constrained. Successive iterations were applied to obtain a better fit to the experimental data. The estimated accuracy of positional parameters is ±0.03 mm s^{-1}. The isomer shift values are referred to SnO_2.

2.5. In-situ, high pressure X-ray photoelectron spectroscopy (XPS)

The in-situ XPS experiments were performed at beam line U49/2-PGM1 of the synchrotron BESSY (Berlin). A pressed pellet containing approximately 150 mg of **PtSn-PS** was placed on a temperature-controlled heater, and treated in-situ in oxygen or hydrogen (0.5 mbar), analogous to treatments of **PtSn-O_2**, and **PtSn-H_2**. Gas flow (15 mL/min) into the reaction cell was controlled using calibrated mass flow controllers.

Sn 3d, O 1s, and Pt 4f spectra were recorded with photon energies of hν = 620 (& 880), 660 (& 920) and 210 (& 470) eV respectively. The different excitation energies on the same core level ensure the variation of information depth, making possible to distinguish between different chemical states as a function of depth. The binding energies were calibrated against the Fermi level of the sample. Decomposition of the Sn 3d and O 1s regions were performed using Gaussian-Lorentzian curves.

2.6. Catalytic tests

Catalytic reactions were carried out in a closed-loop reactor (volume V=155 ml) described earlier [51,53,54]. It was filled with a mixture of the hydrocarbon reactant (1.3 kPa) and hydrogen (16 kPa). Cyclohexene transformation was measured after different treatments in the range of T=353-573 K. Additionally, samples were tested in methylcyclopentane ring opening and in benzene hydrogenation reactions. The same charge of catalyst was used in all test runs, 35 mg of PtSn and 23 mg Pt-black, respectively. Sampling took place after 5-min reaction time in all cases. Product analysis was performed by gas chromatography, using a 50-m CP-Sil glass capillary column. The turnover frequencies [71] were calculated as the number of hexane molecules reacted per one surface Pt atom, using the length of the run as the "contact time". Both samples were pretreated in situ using the treatments described above.

3. Results

3.1. Adsorption properties

The specific surface area measured after presintering was slightly lower for the bimetallic PtSn than for the monometallic Pt sample, 2.31 vs. 2.64 m^2 g^{-1}, respectively (Table 1).

The Pt accessibility ("dispersion") values could only be measured by adsorption techniques after reductive treatments, i.e. presintering and high temperature reduction (Table 1). The values measured were in the range usual for unsupported black samples [52,53]. Treating the unsupported catalyst in oxygen and hydrogen at elevated temperature hardly affected the dispersion pattern, i.e. no sintering occurred. Hydrogen adsorption and CO adsorption gave similar values for monometallic sample, the latter being slightly, but without doubt, higher (Table 1). This difference was much larger for the bimetallic sample, especially after presintering (Table 1). Similar results were obtained

Table 1: Adsorption properties of **PtSn-PS** and **PtSn-H_2** compared to a **Pt** sample after analogous in-situ treatments, noted as **Pt-PS** [69] and **Pt-H_2**.

Catalyst	BET ($m_2\,g^{-1}$)	Dispersion (%)	
		H_2 adsorption	CO adsorption
PtSn-PS	2.31	0.17	0.32
PtSn-H_2	–	0.49	0.56
Pt-PS	2.64	0.89	0.93
Pt-H_2	–	0.85	0.89

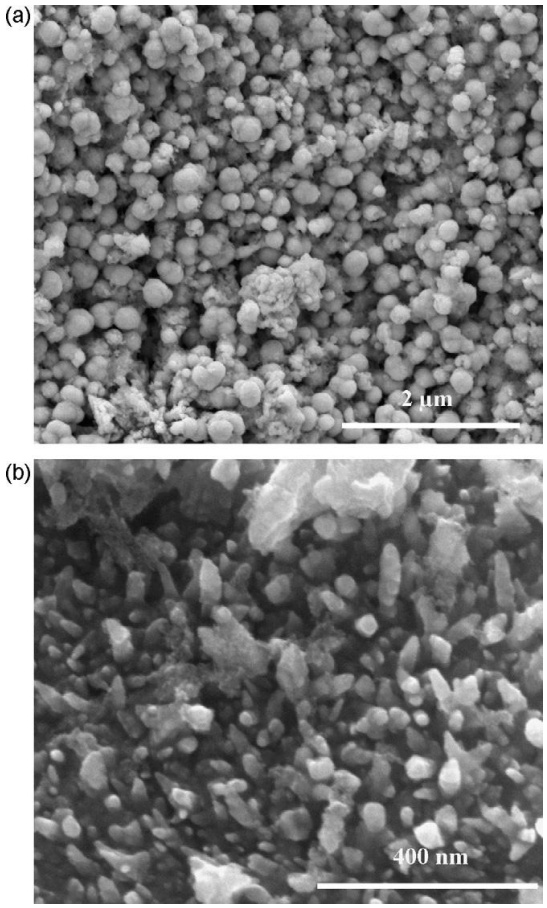

Fig. 1: SEM images of **PtSn-PS**: (a) typical overview, (b) needle-like structures observed on few bigger platelets.

for Pt-Ge [72,73] and Rh-Ge [74,75] – prepared with organometallic grafting – if the loading of the second metal was higher than 1 monolayer. The difference was explained by different site requirements for CO and hydrogen adsorption [73]. The dissociative chemisorption of hydrogen, requires two neighboring active surface sites to dissociate the H_2 molecule. CO (with its lone electron pair) could chemisorb, in turn, upon impinging on a single surface site. These catalysts can contain on the surface single Pt atoms surrounded by the second metal that can apparently adsorb CO in the linear mode, but fewer active doublets are available for H_2 dissociation. We cannot exclude that CO could have been adsorbed on Sn (or SnO – see later) patches. For calculating TOF values, dispersions determined from hydrogen adsorption were used.

Table 2: Phases found by XRD analysis after various treatments

	Component	Proportion (%)
PtSn-AP	Pt	90
	PtSn	0
	Pt_3Sn	10
PtSn-PS	Pt	40
	PtSn	40
	Pt_3Sn	20
PtSn-H_2	Pt	10
	PtSn	0
	Pt_3Sn	90

3.2. Scanning Electron Microscopic (SEM) characterization

Representative Scanning Electron Microscopic pictures of the **PtSn-PS** sample are presented in Figure 1. (TEM analysis of the reference Pt black has been published earlier [76].) Typically, the sample looked like agglomerates of ball-like particles with the size of 50-200 nm (Figure 1a). Hardly any monometallic particle was observed.

In some places larger particles of 1-1.5μm covered by the same ball–like structure was found. In few other places flat plate-like structure covered by needle-like structure of ~40 nm was visible (Figure 1b). The elemental analysis showed homogeneous pattern in this latter case, too, however with higher (over 90%) Pt content.

3.3. Elemental mapping

Elemental mapping was measured on the sample presintered in H_2 at 473 K (**PtSn-H_2**). Figure 2 depicts the elemental maps of selected PtSn particles. It consists of rounded grains: 3 larger ones (up to ~200 nm) are seen together with smaller ones (<50 nm). Sn is situated mainly on the near-surface layers of larger grains, whereas Pt can be found everywhere: on the surface and in deeper layers. Parallel elemental analysis of two grains showed 70-75% Pt and 25-30% Sn (calculated for the whole particles).

3.4. X-ray diffraction analysis

XRD spectra measured in different states are shown in Figure 3 and the corresponding compositions in Table 2. In the **AP** state, after drying, 90% of Pt crystal structure was observed by XRD and only about 10% of crystallized Pt_3Sn was seen (Table 2). The lattice parameter a(0)=3.942 Å was higher than that reported for Pt: (3.9231 Å), indicating dissolution of Sn in the Pt phase, with Sn content of ~6%. The Sn content of the sample estimated from XRD is much lower than the nominal value (Pt:Sn=3:1). Since XRD and SEM also detected more Sn after further treatments, the only possibility is that in the "as prepared" state the missing Sn content is present in an amorphous form, invisible for XRD.

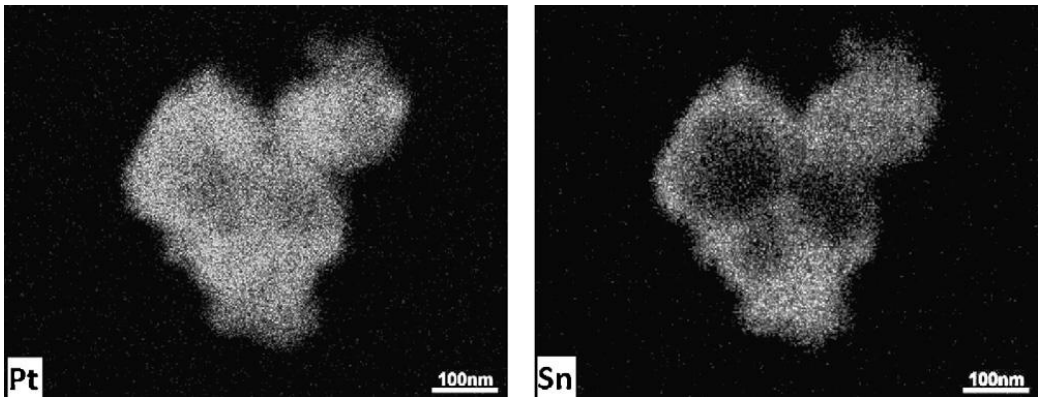

Fig. 2: EDX elemental maps of an agglomerated particle (Pt and Sn).

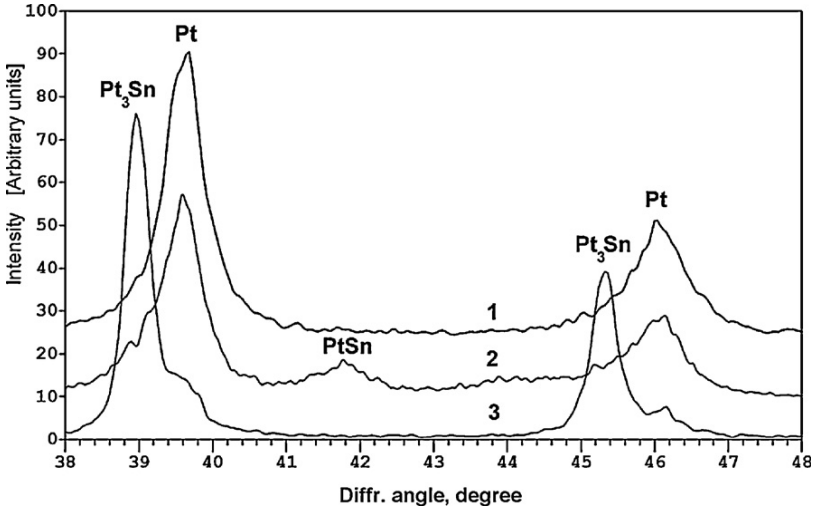

Fig. 3: A section of the X-ray diffractogram of **PtSn** catalyst in three different states: curve 1: **PtSn-AS; curve 2: PtSn-PS; curve 3: PtSn-H_2.** Abscissa: diffraction angle, degrees.

After presintering, a PtSn phase appeared with a concentration of 40%. At the same time, the metallic Pt phase decreased to the same value, and a significant Pt_3Sn phase (20%) also observed (Figure 3 and Table 2). After high temperature O_2 and H_2 treatments, 90% Pt_3Sn was observed with ~10% Pt phase.

3.5. ^{119}Sn-Mössbauer spectroscopy

The Mössbauer spectra are shown in Figure 4 and the calculated fit parameters are presented in Table 3. In the spectrum recorded on the **PtSn-AP** sample, 2/3 of the spectral area belongs to an Sn^{4+} component (with an isomer shift, IS = 0.03 mm/s). Since the isomer shift is related to the Sn^{4+} ($Ba^{119}SnO_3$ source was used), this species is unambiguously Sn^{4+}. The other component at IS=1.27 mm/s, denoted as PtSn (a), can be related to metallic Sn dissolved in Pt, in a concentration around 4-6% [77,78]. Treatment in hydrogen at 473 K resulted in the complete disappearance of the Sn^{4+} state (cf. Section 3.4), with a simultaneous appearance of two new PtSn states: PtSn (b) at 1.41 mm/s and PtSn (c) at 2.05 mm/s. The isomer shift reported for Pt_3Sn is at 1.42 mm/s [26,77,78] corresponding perfectly to PtSn (b). The other compound, PtSn (c) can be regarded as Pt_2Sn_3, but the presence of PtSn cannot be excluded, either (Table 3) [26,77,78].

As expected, oxidizing treatment at 573 K increased the amount of the Sn^{4+} component, however, about 74% of the tin remained in the Pt_3Sn form (Table 3). Finally, after high temperature reduction in H_2, only one component, Pt_3Sn was present in the spectrum of **PtSn-H_2** sample (Figure 4, Table 3).

3.6. In situ, high pressure XPS

The surface state of **PtSn-PS** *during* oxygen treatment as well as in hydrogen treatment was investigated using high-pressure XPS. Gas pressure under the experiment was set to 0.5 mbar. Figure 5 shows the Sn 3d and the O 1s core levels in the different environments, while the Pt

Table 3: Calculated parameters of the Mössbauer spectra shown in Figure 4.

	Component[a]	IS[b]	QS[c]	FWHM[d]	RI[e]
PtSn-AP	Sn^{4+}	0.03	0.53	0.88	67
	PtSn (a)	1.27	–	1.15	33
PtSn-PS	PtSn (b)	1.41	–	1.05	59
	PtSn (c)	2.05	–	1.09	41
PtSn-O_2	Sn^{4+}	0.08	0.71	0.90	26
	PtSn (b)	1.45	–	1.18	74
PtSn-H_2	PtSn (b)	1.48	–	0.99	100

a: Components were identified as follows (see text): PtSn (a): 4-6% Sn dissolved in Pt, PtSn (b): Pt_3Sn, PtSn (c): Pt_2Sn_3.
b: Isomer shift relative to SnO_2 (mm/s)
c: Quadrupole splitting (mm/s)
d: Full line width at half maximum (mm/s).
e: Normalized relative intensity (spectral area, per cent). Because the probability of the Mössbauer effect (recoilless fraction) is different for the various Sn species [77], the RI values do not strictly correspond to the actual concentrations of the respective components.

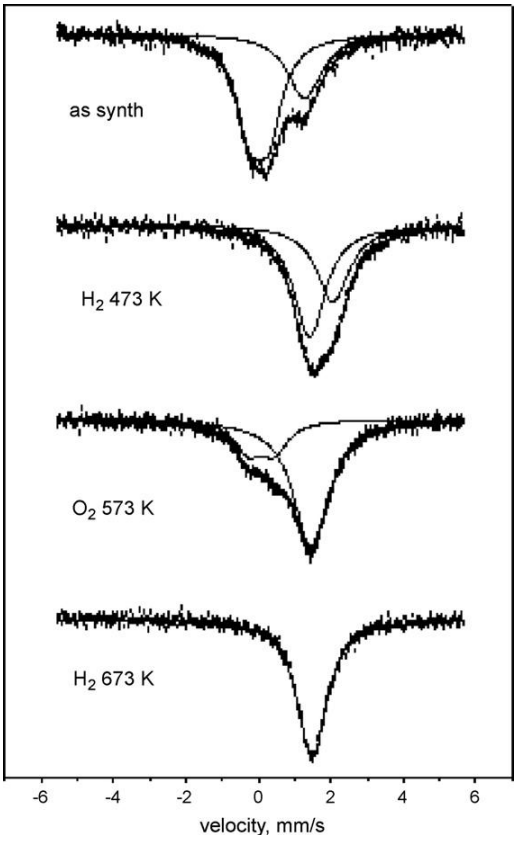

Fig. 4: Series of in situ 77 K Mössbauer spectra recorded on the same sample. Top: **PtSn-AP,** second from top: after treatment in H_2 at 473 K, second from bottom: **PtSn-O_2**, bottom: **PtSn-H_2**.

4f 7/2 peaks are depicted in Figure 6a. The surface of the **PtSn-PS** sample after storing it in air was significantly oxidized. Sn 3d revealed two components slightly overlapping, one at 485.4 and the other at 486.6 eV. As marked on the figure, elemental tin is typically observed at somewhat lower binding energies (484.6-485.0 eV) [79,80], while tin alloyed with Pt would fit the low-BE component [80]. Tin was, in fact, mainly in the form of SnO_2 [79,81], although

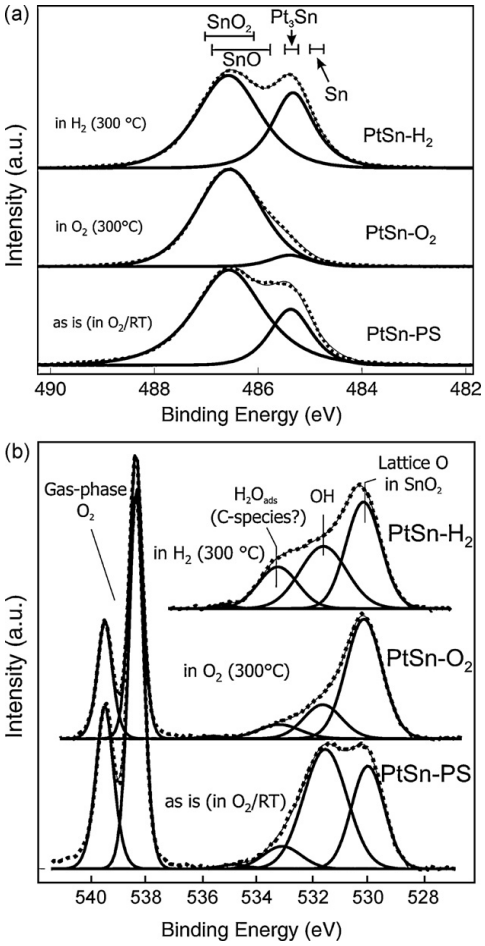

Fig. 5: In situ XP spectra of PtSn in three different states: **PtSn-PS, PtSn-O_2** and **PtSn-H_2**. (a) Sn 3d spectra; (b): O 1s spectra.

the contribution of SnO cannot be excluded as their binding energies are similar [79]. By varying the excitation energy on the same core level, different information depth can be probed. Figure 6b shows such an experiment on the **PtSn-PS** sample after storing it in air. It indicates that SnO_2 is closer to the surface, i.e. more oxide is present on top of the alloyed phase.

The O 1s peak confirmed the presence of 3D tin-oxide, since a pronounced peak of lattice oxygen was present at ~530 eV (Figure 5b). The surface was terminated with hydroxyl groups (531.6 eV) [79,80]. The asymmetry of the high BE side of OH (represented by the 3rd fit curve) can be explained by adsorbed water (not unexpected after sample preparation in aqueous solution and its subsequent treatments with O_2 and H_2). In the **PtSn-PS** state (but also during O_2 or H_2 treatment) the Pt 4f 7/2 level (Figure 6a) is shifted by approximately +0.3 eV as compared to clean Pt (70.9 eV). The Pt 4f 7/2 peak is much broader initially in **PtSn-PS**, which could indicate Pt atoms coordinated with different numbers of tin atoms. The difference spectrum between **PtSn-PS** – **PtSn-H_2** states reveals two additional components at 70.8 and 71.7 eV. While the first can be clean, tin-free platinum the latter resembles the observed core level shift of Cheung [82] for tin–rich samples. Heat

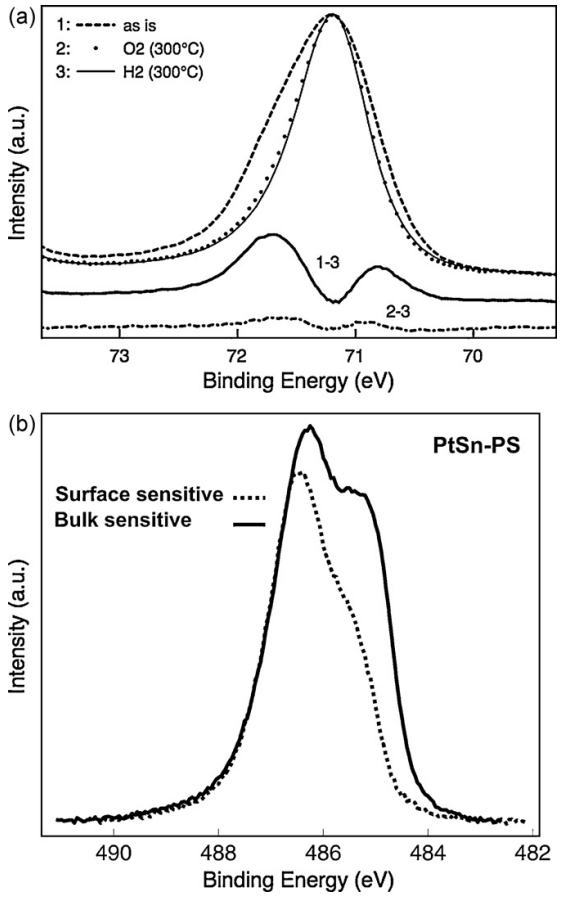

Fig. 6: (a) In situ Pt4f 7/2 peak of PtSn in three different states: **PtSn-PS, PtSn-O_2** and **PtSn-H_2**; (b) Sn 3d depth profiling over **PtSn-PS** (peak BE identifications, see Fig. 5a).

ing in oxygen resulted in a narrower Pt 4f spectrum (Figure 6a); hardly different from the H_2 treated sample. The fraction of SnO_2 also increased (Figure 5a). The onset of the oxide growth was close to 463 K. The high amount of lattice O and the decrease in the number of OH groups points to a 3D growth of tin-oxide (tin migrating to the surface where it gets oxidized) as well as to the lower stability of hydroxyls.

The ratio Sn/Pt as measured by XPS increased from 4 to more than 10 as a result of heating in oxygen, validating the above results. During heating some oxygen containing carbon species (not shown) segregated to the surface (and was stable at 573 K). These entities could also contribute to the component of the O 1s peak at ~ 531.6 eV, attributed mainly to OH groups (Figure 5b).

Hydrogen treatment at 573 K reduced the amount of SnO_2 and platinum segregated to the surface. The ratio of Sn/Pt dropped by a factor of almost 6; thus platinum migrated from bulk towards the surface. The narrowest Pt 4f was observed in this state (Figure 6a), suggesting only one type of Pt being present, with BE close to that of metallic Pt [50,53]. This was further confirmed by a depth profiling experiment (not shown), revealing no emerging new component next to the main Pt 4f peak. Sn 3d of the alloy component was better resolved in H_2 and its BE corresponded to that of Pt_3Sn [79]. The amount of tin oxide was remarkable in both Sn 3d and O 1s-core levels (Figure 5). Hydrogen induced the formation of hydroxyls and adsorbed wawater.

3.7. Catalytic studies

The Pt-Sn samples after any of the treatments were inactive in methyl-cyclopentane ring opening reaction (in the range of T=543-603 K) and benzene hydrogenation (T=353-473 K). The same charge of catalyst was, however, active in cyclohexene transformation (T=353-573 K), producing benzene and cyclohexane:

$$C_6H_{12} \xleftarrow{+H_2} C_6H_{10} \xrightarrow{-2H_2} C_6H_6$$

Pt black (**Pt**) was active in all reactions. The poor activity in the above mentioned reactions indicates (i) that Pt-Sn phases are inactive in the C–C cleavage and in the saturation of aromatic ring and/or (ii) a strong geometric hindrance of the adsorption of $C_5 – C_6$ carbocycles.

The conversion values in cyclohexene transformation measured after different treatments on PtSn are presented in Figure 7a in comparison with **Pt** catalyst, subjected also to analogous pretreatments: O_2 and O_2–H_2, respectively. These latter results corresponded perfectly with those shown on the presintered sample. Thus, the effect of pretreatments on the catalytic behavior of PtSn can only be correlated with presence of Sn. Among the Sn containing samples, the activity was the highest on **PtSn-H_2** and lowest on the presintered sample. The activity pattern after oxygen treatment resembled that of the latter sample, both increasing at T>473 K. These samples were treated in H_2 at T=473 K after preparation (**Pt-PS**) as well as after oxidation (**Pt-O_2**) in order to remove residual surface oxygen from Pt. These catalysts contacted first hydrogen at T > 473K, during the reaction. Hydrogen increased the number of available surface Pt atoms, as seen from XPS measurements (see Section 3.5), increasing also the activity.

The activity measured on **Pt-PS** decreased continuously and on **PtSn-H_2** decreased after a maximum at T=393 K. Cyclohexene formed two products: cyclohexane and benzene. The reactions include hydrogenation and dehydrogenation. Dehydrogenation of cyclohexene to benzene was, likely, "structure-sensitive" [83], i.e., just certain catalytic sites with threefold symmetry were active for this process. Hydrogenation of cyclohexene, in turn, was found to be "structure-insensitive" [84] – i.e., its active sites consisting of one or two Pt atoms could be anywhere of the active surface.

The compositions reported are far from equilibrium: the real equilibrium mixture containing negligible amount of cyclohexene. Cyclohexane prevails below ~573 K and benzene above that temperature [73]. The rates for the production of these molecules (expressed as TOF values) are compared for **Pt-PS** and **PtSn-H_2** in Figure 7b. Benzene

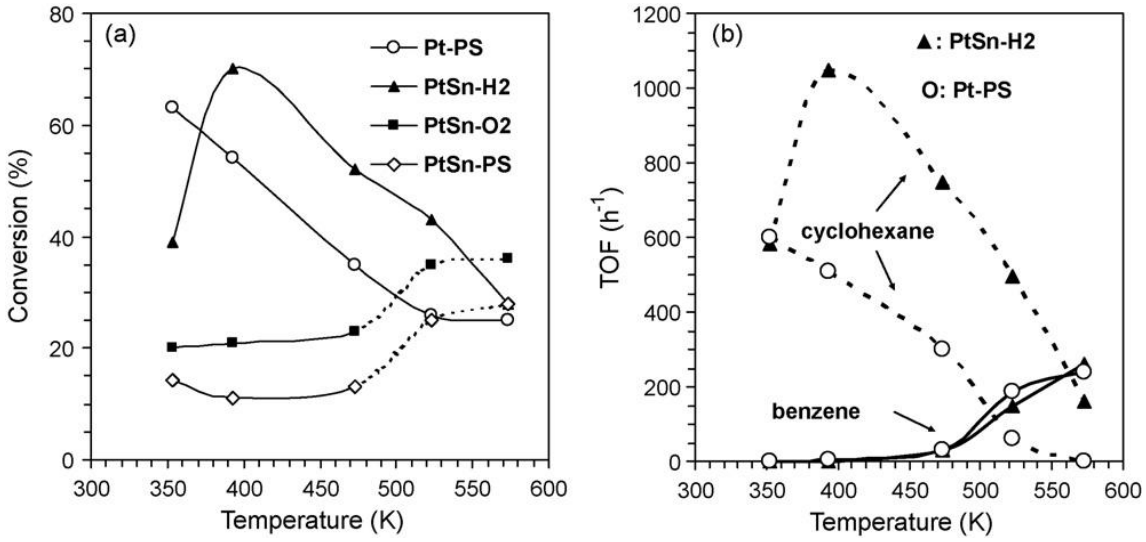

Fig. 7: (a) Conversion of cyclohexene on Pt and PtSn catalysts after different pretreatments and (b) turnover frequencies (TOF) for the formation of benzene and cyclohexane on Pt and on hydrogen treated PtSn.

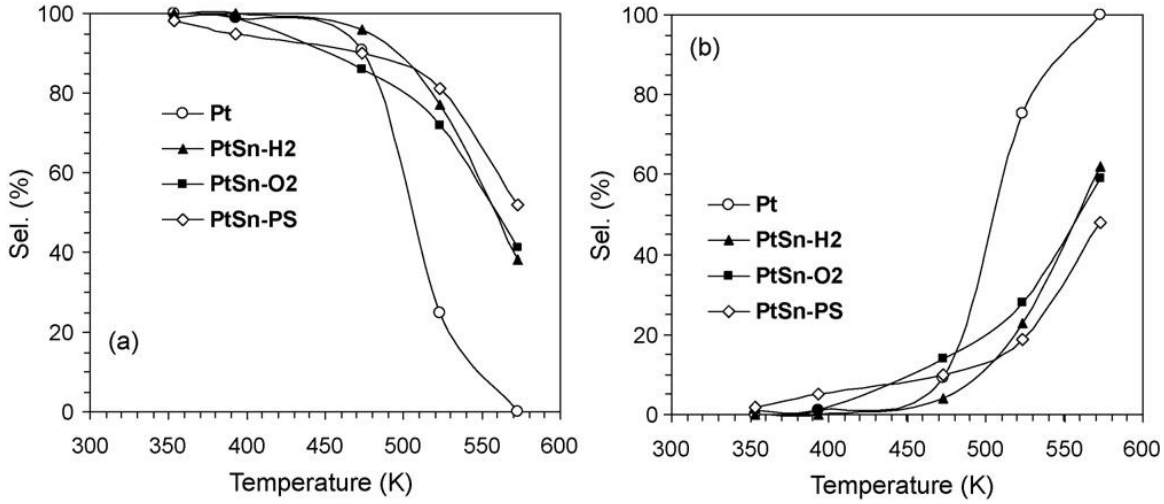

Fig. 8: Selectivity pattern of (a) cyclohexane and (b) benzene formation over Pt and PtSn after different pretreatments as a function of temperature.

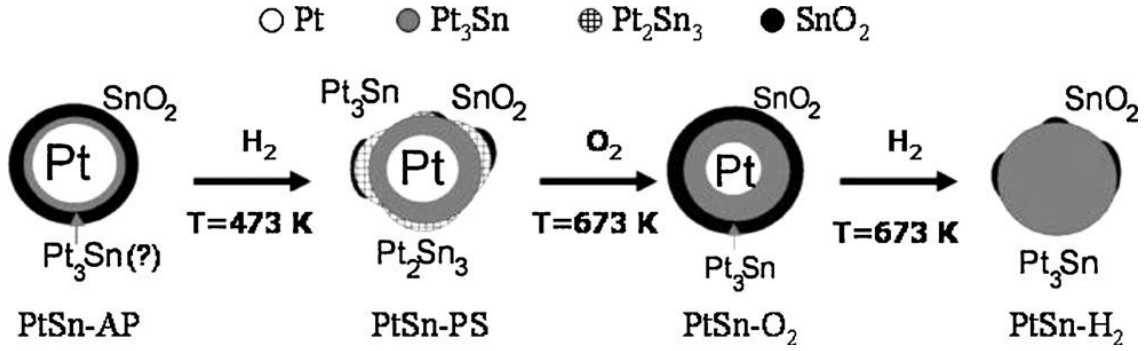

Fig. 9: Schematic model of solid-state transformations after different pretreatments. The approximate area of components agrees qualitatively with the values of Table 3. The question mark after Pt_3Sn in **PtSn-AP** means that it is not detected as a phase (Table 3), but its formation may have started from dissolved Sn in Pt.

formation was the same on both samples, indicating strong thermodynamic control of its formation [73]. The activity difference between the two samples is caused by the higher reaction rate towards cyclohexane formation from cyclohexene on PtSn. The higher hydrogenation activity of PtSn samples is also manifested in the selectivity values (Figure 8). The abundance of benzene and cyclohexane as a function of the temperature were determined first of all, by thermodynamics. Nevertheless, the amount of cyclohexane measured after reaction in the gas phase was always somewhat larger, that of benzene smaller that predicted by the equilibrium which was usually approximated, but never reached, like reported in our earlier paper [73]. Two factors may be important: first, the few minutes of reaction were not sufficient to establish an equilibrium mixture (the transformation of cyclohexene was much less than 100%); second, the hydrogen concentration in the surface phase – where the actual reaction took place – was pronouncedly different from that observed in the gas phase. It was just the measured product distribution that allowed calculating the "effective surface hydrogen pressures" being higher than the values measured in the gas phase [85].

4. Discussion

The "multiplet theory" of catalysis [86] predicts that active sites for hydrocarbons with C_6 ring comprise of three-atom Pt sites in hexagonal conformation: (111) planes, edges, and kinks with such symmetry [87]. Added inactive components (Sn [5] and/or Ge [72]) could preserve these active ensembles, and prevent the formation of contiguous carbonaceous overlayer. Too much additive could deactivate reactions requiring "sextet-type" active ensembles, but "doublets" remained still active. Thus, benzene could not be hydrogenated on extremely sulfided Pt, but cyclohexene was readily hydrogenated [88]. Similar activity loss was observed with much Ge added to Pt/Al_2O_3, transforming small Pt particle into "bulk" PtGe grains of the same size on the support [72]. The analogy can be valid in this case of larger grains in the present study.

Solid-state transformations of our binary system as a consequence of various treatments were followed (Tables 1 and 2). Adding Sn produced some Pt_3Sn on the surface, at the same time, SnO_2 was also formed. Sn enrichment took place in near-surface regions after first sintering (**PS**). In this state some PtSn was present (Figure 3). A subsequent O_2 treatment, in turn, brought about mixed phases and, at the same time, lowered the catalytic activity (Figure 7a). The last H_2 treatment at 673 K transformed ~90% of Pt to Pt_3Sn (detected also by XRD, Figure 3). Figure 9 depicts schematically these solid-state transformations. This scheme – constructed on the basis of phase analysis – suggests the same conclusion as drawn from the elemental map shown (Figure 2): Sn is accumulated in near-surface positions. This is in fair agreement also with a previous study with $PtSn/Al_2O_3$ [48] reporting increasing amounts of Sn^{4+} and Sn^0 upon repeated treatments. A parallel higher activity was also reported in propane dehydrogenation [48].

The overall catalytic activity (Figure 7) was high on monometallic **Pt-PS**. The formation of PtSn after first sintering of the bimetallic sample (**PtSn-PS**) decreased the activity. This alloy would contain hardly any surface Pt ensembles necessary for catalysis [11]. After the final treatment: **PtSn-H_2**, transforming the major part of the grains into Pt_3Sn, the catalyst was more active than the monometallic **Pt-PS**, like with bimetallic RhSn [89] and PtGe [73], containing lower amounts of the second metal. This manifested itself mainly at lower temperatures and produced first of all, cyclohexane, meaning almost pure "doublet" reactions (Figure 7b) as expected from a binary alloy (lacking Pt "sextets" on its surface). Our catalyst (Figure 7) was analogous to $PtSn/Al_2O_3$ prepared by coimpregnation exhibiting much lower activity than $PtSn/Al_2O_3$ prepared by consecutive impregnation [11]. The selectivities of all **Pt-Sn** catalysts were rather similar (Figure 8), indicating a different number, but similar active sites. "Sextet" reaction (producing up to 100% benzene) was observed on **Pt** (Fig. 7). Aromatization must have occurred via a "stepwise" route (cyclohexene → cyclohexadiene → benzene [90]) on alloy catalysts. To sum up – although Pt_3Sn proved to be active in cyclohexene transformation (even to benzene) – this may be due to the structure of this alloy exposing some triangular Pt ensembles on its (111) plane [11]. Still, the selectivities (Figure 8) gave evidence on the superiority of **Pt** surface (without Sn) in aromatization.

Acknowledgement

The authors are grateful to Mr Norbert Pfänder for the EDX measurements. A. W. thanks the support from the Hungarian Science Foundation (OTKA Grant No NF 73241) for financial support.

References

[1] V. Ponec G. C. Bond, Catalysis by Metals and Alloys, Stud. Surf. Sci. Catal. Vol. 95, Elsevier, Amsterdam, 1995.
[2] V. Ponec, Adv. Catal. 32 (1983) 149–214.
[3] J. H. Sinfelt, Bimetallic Catalysts: Discoveries, Concepts and Applications, Wiley, New York, 1983.
[4] B. H. Davis, J. Catal. 42 (1976) 376–380.
[5] F. M. Dautzenberg, J. N. Helle, P. Biloen, W. M. H. Sachtler, J. Catal. 63 (1980) 119–128.
[6] T. Fujikawa, F. H. Ribeiro, G.A. Somorjai, J. Catal., 178 (1998) 58–65.
[7] F. Epron, C. Carnevillier, P. Marécot, Appl. Catal. A 295 (2005) 157–169.

[8] B. H. Davis, Catal. Today 53 (1999) 443–516.
[9] M. P. González-Marcos, B. Iñarra, J. M. Guil, M. A. Gutiérrez-Ortiz, Appl. Catal. A 273 (2004) 259–268.
[10] Z. Paál, A. Győry, I. Uszkurat, S. Olivier, M. Guérin, C. Kappenstein, J. Catal. 168 (1997) 164–175.
[11] C. Kappenstein, M. Guérin, K. Lázár, K. Matusek, Z. Paál, J. Chem. Soc. Faraday Trans. 94 (1998) 2463–2473.
[12] K. Matusek, C. Kappenstein, M. Guérin, Z. Paál, Catal. Lett. 64 (2000) 33–36.
[13] G. J. Siri, J. M. Ramallo-López, M. L. Casella, J. L. G. Fierro, F. G. Requejo, O. A. Ferretti, App. Catal. A 278 (2005) 239–249.
[14] J. Salmones, J.-A. Wang, J. A., Galicia, G. Aguilar-Rios, J. Mol. Catal. A 184 (2002) 203–213.
[15] O. A. Bariås, A. Holmen, E. A. Blekkan J. Catal. 158 (1996) 1–12.
[16] H. Zhao, B. E. Koel, J. Catal. 234 (2005) 24–32.
[17] J.L. Margitfalvi, I. Borbáth, M. Hegedűs, A. Tompos, Appl. Catal. A 229 (2002) 35–49.
[18] J.M. Ramallo-López, G. F. Santori, L. Giovanetti, M. L. Casella, O. A. Ferretti, F. G. Requejo, J. Phys. Chem. B 107 (2003) 11441–11451.
[19] S. Göbölös, N. Mahata, I. Borbáth, M. Hegedűs, J. L. Margitfalvi, React. Kinet. Catal. Lett. 74 (2001) 345–352.
[20] G. Corro, R. Montiel, J. Mol. Catal. 184 (2002) 443–449.
[21] K. Lázár, W. D. Rhodes, I. Borbáth, M. Hegedűs, J. L. Margitfalvi, Hyperfine Interactions 139/140 (2002) 87–96.
[22] W. D. Rhodes, K. Lázár, V. I. Kovalchuk, J. L. d'Itri, J. Catal. 211 (2002) 173–182.
[23] W. D. Rhodes, J. L. Margitfalvi, I. Borbáth, K. Lázár, V. I. Kovalchuk, J. L. d'Itri, J. Catal. 230 (2005) 86–97.
[24] J.L. Margitfalvi, I. Borbáth, M. Hegedűs, A. Szegedi, K. Lázár, S. Göbölös, S. Kristyán, Catal. Today 73 (2002) 343–353.
[25] J. L. Margitfalvi, I. Borbáth, M. Hegedűs, E. Tfirst, K. Lázár, J. Catal. 196 (2000) 200–204.
[26] J. L. Margitfalvi, I. Borbáth, K. Lázár, E. Tfirst, A. Szegedi, M. Hegedűs, S. Gőbölös, J. Catal. 203 (2001) 94–103.
[27] A. N. Akin, G. Kilaz, A. I. Işli, Z. I. Önsan, Chem. Eng. Sci. 56 (2001) 881–888.
[28] A. E. Aksoylu, M. MAdalena, A. Freitas, J. L. Figueiredo, Catal. Today 62 (2000) 337–346.
[29] M. M. Schubert, M. J. Kahlich, G. Feldmeyer, M. Hüttner, S. Hackensberg, H. A. Gasteiger, R. J. Behm, Phys. Chem. Chem. Phys. 3 (2001) 1123–1131.
[30] S. Özkara, A. E. Aksoylu, Appl. Catal. A 251 (2003) 75–83.
[31] P. Marques, N. F. P. Ribeiro, M. Schmal, D. A. G. Aranda, M. V. M. Souza, J. Power Sources 158 (2006) 504–508.
[32] I. Honna, T. Toda, J. Electrochem. Soc. 150 (2003) A1689–A1692.
[33] K. Wang, H. A. Gasteiger, M. M. Markovic and P. N. Ross Jr, Electrochimica Acta 41 (1996) 2587–2593.
[34] J.-M. Léger, S. Rousseau, C. Countanceau, F. Hahn, C. Lamy, Electrochimica Acta 50 (2005) 5118–5125.
[35] H. Wang, Z. Jusys, R. J. Behm, J. Power Sources, 154 (2006) 351–359.
[36] M. Arnez, V. Stamenkovic, B. B. Blizanac, K. J. Mayrhofer, N. M. Markovic, P. N. Ross, J. Catal. 232 (2005) 402–410.
[37] G. Avgouropoulos, T. Ionnides, Appl. Catal. B. Env. 56 (2005) 77–86.
[38] G. Maitzner, G. H. Via, F. W. Lytle, S. C. Fung, J. H. Sinfelt, J. Phys. Chem. 92 (1988) 2925–2932.
[39] Y. X. Li, K. J. Klabunde, J. Catal., 126 (1990) 173–186.
[40] H. Verbeek, W. M. H. Sachtler, J. Catal. 42 (1976) 257–267.
[41] R. Burch, J. Catal. 71 (1981) 348–357.
[42] A. Palazov, Ch. Bonev, D. Shopov, G. Lietz, A. Sárkány, J. Völter, J. Catal. 103 (1987) 249–260.
[43] E. Grantscharova-Anderson, A. B. Anderson, Electrochimica Acta 44 (1999) 4543–4550.
[44] E. Lamy-Pitara, L. El Ouazzani-Benhima, J. Barbier, M. Cahoreau, J. Caisso, Appl. Catal. A 81 (1992) 47–65.
[45] Ph. Durussel, R. Massara, P. Feschotte, J. Alloys Comp. 215 (1994) 175–179.
[46] P. Anres, M. Gaune-Escard, J. P. Bross, E. Hayer, J. Alloys Comp. 280 (1998) 158–167.
[47] A. Sümer, M. A. Gülem, A. E. Aksolyu, Surf. Sci. 600 (2006) 2026–2039.
[48] W. Yang, L. Li, Y. Fan, J. Zang, Catal. Lett., 12 (1992) 267–275
[49] Z. Paál, Zh. Zhan, E. Fülöp, B. Tesche, J. Catal., 156 (1995) 19–27.
[50] Z. Paál, R. Schlögl, G. Ertl, J. Chem. Soc. Faraday Trans. 88 (1992) 1179–1189.
[51] N. M. Rodriguez, P. E. Anderson, A. Wootsch, U. Wild, R. Schlögl, Z. Paál, J. Catal., 197 (2001) 365–377.
[52] J. Find, Z. Paál, R. Schlögl, U. Wild, Catal. Lett. 65 (2000) 19–23.
[53] Z. Paál, U. Wild, A. Wootsch, J. Find, R. Schlögl, Phys. Chem. Chem. Phys. 3 (2001) 2148–2155.
[54] Z. Paál, A. Wootsch, Catalysis in Application (Ed. S. D. Jackson, J. S. J. Hargreaves, D. Lennon,) The Royal Soc. Chemistry, Cambridge, 2003, p. 8–15.
[55] R. W. Joyner, M. W. Roberts, Chem. Phys. Lett. 60 (1979) 459–462.
[56] G. A. Somorjai, G. Rupprechter, J. Phys Chem. B 103 (1999) 1623–1638.
[57] F. Garin, G. Maire, S. Zyade, M. Zauwen, A. Frennet, P. Zielinski, J. Mol. Catal. 58 (1990) 185–197.
[58] H. Bluhm, M. Hävecker, A. Knop-Gericke, E. Kleimenov, R. Schlögl, D. Teschner, V. I. Bukhtiyarov, D. F. Ogletree, M. Salmeron, J. Phys. Chem. B 108 (2004) 14340–14347.
[59] V. V. Kaichev, I. P. Prosvirin, V. L. Bukhtiyarov, H. Unterhalt, G. Rupprechter,
    a. H.-J. Freund, J. Phys. Chem. B. 107 (2003) 3522–3527.
[60] V. I. Bukhtiyarov, I. P. Prosvirin, E. P. Tikhomirov, V. V. Kaichev, A. M. Sorokin, V. V. Evstigneev, React. Kinet. Cat. Lett. 79 (2003) 181–188.
[61] V. I. Bukhtiyarov, Kinet. Catal. 44 (2003) 420–431.
[62] H.-J. Ruppender, M. Grunze, C. W. Kong, M. Wilmers, Surf. Interface Anal. 15 (1990) 245–253.
[63] D. Teschner, A. Pestryakov, E. Kleimenov, M. Hävecker, H. Bluhm, H. Sauer, A. Knop-Gericke, R. Schlögl: J. Catal., 230 (2005) 186–194.
[64] D. Teschner, A. Pestryakov, E. Kleimenov, M. Hävecker, H. Bluhm, H. Sauer, A. Knop-Gericke, R. Schlögl: J. Catal., 230 (2005) 195–203.
[65] O. Pozdnyakova, D. Teschner, A. Wootsch, J. Kröhnert, B. Steinhauer, H. Sauer, L. Toth, F. C. Jentoft, A. Knop-Gericke, Z. Paál, R. Schlögl, J. Catal. 237 (2006) 1–16.
[66] O. Pozdnyakova, D. Teschner, A. Wootsch, J. Kröhnert, B. Steinhauer, H. Sauer, L. Toth, F. C. Jentoft, A. Knop-Gericke, Z. Paál, R. Schlögl, J. Catal. 237 (2006) 17–28.
[67] D. Teschner, A. Wootsch, O. Pozdnyakova, H. Sauer, A. Knop-Gericke, R. Schlögl, React. Kinet. Catal. Lett. 87 (2006) 235–247.
[68] C. Paal, Berichte 49 (1916) 548–560.
[69] A. Wootsch, Z. Paál, J. Catal. 205 (2002) 86–96.
[70] K. Lázár, Struct. Chem. 2 (1991) 245–265.

[71] M. Boudart, *in* "Handbook of Heterogeneous Catalysis" (G. Ertl, H. Knözinger and J. Weitkamp, Eds.) Vol. 3, p. 958–972.Verlag Chemie, Weinheim, 1997.
[72] A. Wootsch, L. Pirault-Roy, J. Leverd, M. Guérin, Z. Paál, J. Catal, 208 (2002) 490–493.
[73] A. Wootsch, Z. Paál, N. Győrffy, S. Ello, I. Boghian, J. Leverd, L. Pirault-Roy., J. Catal. 238 (2006) 67–78.
[74] L. Pirault-Roy, D. Teschner, Z. Paál, M. Guérin, Appl. Catal. A 245 (2003) 15–31.
[75] D. Teschner, L. Pirault-Roy, D. Naud, M. Guérin, Z. Paál, Appl. Catal. A 252 (2003) 421–426.
[76] Z. Paál, A. Wootsch, I. Bakos, S. Szabó, H. Sauer, U. Wild¸ R. Schlögl, Appl. Catal. A. 309 (2006) 1–9.
[77] N.N. Greenwood and T.C. Gibb, Mössbauer Spectroscopy, Chapman–Hall, London (1971).
[78] M.C. Hobson, S. L. Goresh G. P. Khare, J. Catal. 142 (1993) 641–654.
[79] J. Chastain (Ed.), Handbook of X-ray Photoelectron Spectroscopy, Perkin-Elmer, 1992.
[80] S. D. Gardner, G. B. Hoflund, D. R. Schryer, J. Catal. 119 (1989) 179–186.
[81] A. W. C. Lin, N. R. Armstrong, T. Kuwana, Anal. Chem. 49 (1977) 1228–1235.
[82] T. T. P. Cheung, Surf. Sci. 177 (1986) 493–514.
[83] M. Boudart, Adv. Catal., 20 (1969) 153–166.
[84] R. M. Rioux, B. B. Hsu, M. E. Grass, H. Song, G. A. Somorjai, Catal. Lett., 126 (2008) 10–19.
[85] Z. Paál, G. Székely, P. Tétényi, J. Catal. 58 (1971) 108–113.
[86] A. A. Balandin, Adv. Catal. 19 (1969) 1–210.
[87] S.M. Davis, F. Zaera, G.A. Somorjai, J. Catal. 85 (1984) 206–223.
[88] M.-D. Appay, J.-M. Manoli, C. Potvin, M. Muhler, U. Wild, O. Pozdnyakova, Z. Paál, J. Catal. 222 (2004) 419–428.
[89] M. Chamam, K. Lázár, L. Pirault-Roy, I. Boghian, Z. Paál, A. Wootsch, Appl. Catal. A, 332 (2007) 27–36.
[90] P. Tétényi, in Surface and Defect Properties of Solids, Spec. Periodical Reports (M.W. Roberts, J. J. Thomas, Eds), The Chemical Society, London, 1976, Vol.5, 81–102.